

# Universal Event Detection in Time Series

1<sup>st</sup> Menouar Azib *Akkodis, France*

menouar.azib@akkodis.com 2<sup>nd</sup> Benjamin Renard *Akkodis, France*

benjamin.renard@akkodis.com 3<sup>rd</sup> Philippe Garnier *Université de Toulouse, France*

philippe.garnier@irap.omp.eu 4<sup>th</sup> Vincent Génot *Université de Toulouse, France*

vincent.genot@irap.omp.eu 5<sup>th</sup> Nicolas André *Université de Toulouse, France*

nicolas.andre@irap.omp.eu

**Abstract**—In our previously published work, we introduced a supervised deep learning method for event detection in multivariate time series data, employing regression instead of binary classification. This simplification avoids the need for point-wise labels throughout the entire dataset, relying solely on ground truth events defined as time points or intervals. In this paper, we establish mathematically that our method is universal, capable of detecting any type of event with arbitrary precision under mild continuity assumptions on the time series. These events may encompass change points, frauds, anomalies, physical occurrences, and more. We substantiate our theoretical results using the universal approximation theorem for feed-forward neural networks (FFN). Additionally, we provide empirical validations that confirm our claims, demonstrating that our method, with a limited number of parameters, outperforms other deep learning approaches, particularly for rare events and imbalanced datasets from different domains.

**Index Terms**—Event Detection in Multivariate Time Series, Universal Approximations, Feed-Forward Neural Networks, Deep Learning, Supervised Learning

## I. INTRODUCTION

IN the domain of time series analysis, event detection is concerned with the identification of significant deviations, which extend beyond merely change points and anomalies. It’s noteworthy that the majority of research in event detection has been predominantly centered on change point detection and anomalies. Change point detection is primarily concerned with instances where a shift in statistical properties is observed. Put simply, given a time series, the aim is to identify the points at which a significant change takes place. On the contrary, anomalies are data points that markedly deviate from the expected trend. In relation to a time series, the objective is to locate the instances that correspond to an unusual event. However, event detection encompasses a broad array of significant changes in time series data such as frauds and physical events.

A multitude of supervised deep learning methods have been devised to tackle the challenges inherent in detecting change points and anomalies in time series data. These methods leverage the capabilities of deep learning to discern intricate patterns and dependencies within the data, thereby enabling more precise and robust detection.

These methods can be broadly classified into two main categories: The first category comprises primarily empirical

methods that focus on practical applications and performance on benchmark datasets, without an accompanying theoretical discourse [1]–[18]. The second category encompasses methods that include a theoretical discussion about the universality of the approach being developed. These methods typically offer mathematical proofs or theoretical justifications for their efficacy. To our knowledge, one work, [19], belongs to this category.

In the study by [19], the authors propose a novel change point detection method that utilizes a neural network. This architecture includes the CUSUM-based classifier [20] as a specific instance. The authors demonstrate that this architecture cannot underperform the CUSUM classifier in identifying change points. They also show that the misclassification error is constrained by two factors: one associated with the inherent misclassification error of the CUSUM-based classifier, and another related to the complexity of the neural network class as gauged by its Vapnik-Chervonenkis (VC) dimension [21]. However, this study has certain limitations. It models this problem as a change-in-mean model [22], which may not be adequately generalized for other types of event detection, including anomalies. Moreover, it assumes that the data are drawn from a multivariate normal distribution. This assumption may not universally hold true for all types of time series data, potentially limiting the applicability of their approach.

In our prior work [23], we introduced a unique supervised deep learning approach for detecting events in multivariate time series data. Our method employs regression instead of binary classification and requires only the ground truth events—defined as specific time points or intervals—eliminating the need for point-wise labels across the entire dataset.

In this paper, we present a comprehensive theoretical analysis of our event detection method. We demonstrate its universality under mild assumptions regarding the continuity of a multivariate time series and establish that our approach can detect a broad spectrum of events with arbitrary precision. This assertion is grounded in the universal approximation theorem [24], emphasizing the robust theoretical foundations of our method. Notably, our method stands out for its robustness and broader applicability compared to [19], as it is not limited to change point detection and imposes weaker assumptions. This nuanced approach enhances the versatility of our method, making it suitable for diverse scenarios in event detection.

Beyond the theoretical aspects, we also demonstrate the

practical effectiveness of our approach. Despite having a minimal number of trainable parameters, our method surpasses existing deep-learning techniques when applied to real-world imbalanced datasets, such as those used in fraud detection and bow shock crossing identification. These empirical validations highlight not only the efficacy but also the applicability of our method across a range of domains, thereby positioning it as a strong contender in the field of event detection across various disciplines.

## II. MATHEMATICAL FORMULATION

This section introduces the mathematical formulation of our method. The method is based on two key components: a multivariate time series that represents the dataset, and a set of reference events, also known as ground truth events. Let  $T(t)$  be a time series that maps a real value  $t$  to a feature vector in  $\mathcal{X} \subset \mathbb{R}^f$ , where  $f$  is the number of features. The mapping can be represented as follows:

$$T: \mathbb{R} \rightarrow \mathcal{X} \subset \mathbb{R}^f \\ t \mapsto T(t)$$

The ground truth events are encapsulated within a set  $E$ . Each event  $e$  within this set is an interval defined by a start time  $\tau_1$  and an end time  $\tau_2$ , denoted as  $e = [\tau_1, \tau_2]$ , where both  $\tau_1$  and  $\tau_2$  are real numbers. We assume, without loss of generality, that the time series  $T(t)$  is defined for all  $t$  in the interval  $[\alpha, \beta]$ , where  $\alpha$  and  $\beta$  are real numbers, and that it takes values in  $\mathcal{X}$ . Additionally, we assume that the reference events in the set  $E$  do not overlap, i.e., for all  $e_1, e_2 \in E$ , the intersection of  $e_1$  and  $e_2$  is an empty set ( $e_1 \cap e_2 = \emptyset$ ).

### A. Overlapping Partitions

In this subsection, we explain the concept of overlapping partitions. We split the interval  $[\alpha, \beta]$  into a sequence of equally spaced points ( $t_1 = \alpha < t_2 < t_3, \dots < t_N = \beta$ ), where  $N \in \mathbb{N}$ , and the spacing is  $s \in \mathbb{R}$ . We consider a family of overlapping partitions  $(p_i)_{i \in I}$  where  $I = \{i \in \mathbb{N} | 1 \leq i \wedge i \leq N - w + 1\}$  is an index set. An overlapping partition  $p_i$  is set of size  $w \in \mathbb{N}, w > 1$ , denoted by  $\{t_i, t_{i+1}, \dots, t_{i+w-1}\}$ , where  $i$  is in  $I$ . The set of all overlapping partitions is  $\mathcal{P} = \{p_i | i \in I\}$ . The term 'overlapping' means that any two neighboring partitions have at least one point in common. Next, we define a function  $o$  that maps each overlapping partition  $p_i \in \mathcal{P}$  to a vector  $v_i \in \mathcal{V}$ , as follows:

$$o: \mathcal{P} \rightarrow \mathcal{V} \\ p_i \mapsto v_i = o(p_i)$$

Here  $\mathcal{V} = \{o(p_i) | i \in I\}$ . The function  $o$  assigns to the partition  $p_i$  a vector  $v_i$  of dimension  $r = w \cdot f$ , which contains the values

of the time series  $T(t_j)$  for all  $j$  such that  $i \leq j \wedge j \leq i+w-1$ . The vector  $v_i$  can be written as follows:

$$v_i = \begin{pmatrix} T(t_i)[1] \\ \vdots \\ T(t_i)[f] \\ \vdots \\ T(t_{i+w-1})[1] \\ \vdots \\ T(t_{i+w-1})[f] \end{pmatrix}$$

This representation concatenates the feature values of the time series  $T$  over the partition  $p_i$ , where  $T(t_j)[k]$  denotes the  $k$ -th feature value at time  $t_j$ .

### B. Overlapping Parameter Function

In this subsection, we introduce the overlapping parameter function, denoted as  $op$ , which quantifies the temporal distance of each partition  $p_i \in \mathcal{P}$  with respect to the nearest events. The function  $op$  assigns a value between 0 and 1 to each partition.

To calculate the  $op$  value for a given event  $e \in E$  and partition  $p_i \in \mathcal{P}$ , we use the Jaccard similarity coefficient [25]. The  $op$  value is computed by taking the duration of the intersection between  $p_i$  and  $e$ , and dividing it by the duration of their union. This is shown in the following formula:

$$op(p_i, e) = \frac{\text{duration}(p_i \cap e)}{\text{duration}(p_i \cup e)} \quad (1)$$

The value of  $op(p_i, e)$  will be close to 1 if the event  $e$  and the partition  $p_i$  largely overlap, and close to 0 if they have little overlap. This provides a measure of the temporal proximity of the partition to the event.

Given that the cardinality of each partition is denoted as  $w$ , we define the temporal duration  $w_s$  as  $w_s = (w - 1) \cdot s$ . To synchronize the temporal duration of each partition ( $w_s$ ) with the events, we adjust each event  $e$  using the following formula:

$$\forall e = [\tau_1, \tau_2] \in E, \\ t_{mid} = \frac{\tau_1 + \tau_2}{2}, \\ e = \left[ \tau_{mid} - \frac{w_s}{2}, \tau_{mid} + \frac{w_s}{2} \right]$$

This formula modifies the start and stop times of each event to align with the temporal size of the partitions. The midpoint of the event remains the same, but the duration is adjusted to match  $w_s$ .

**Definition 1.** Let  $p_i = \{t_i, t_{i+1}, \dots, t_{i+w-1}\}$ , where  $i \in I$ , be a partition. The event  $e = [\tau_1, \tau_2]$ , where  $e \in E$ , is considered close to  $p_i$  if:

$$|t_i - \tau_1| < \frac{w_s}{2}.$$

**Definition 2.** Given  $p_i$  and  $e = [\tau_1, \tau_2] \in E$ , with  $t_{i+w-1} = t_i + w_s$ , we define  $p_i \cap e$  and  $p_i \cup e$  as follows:

$$p_i \cap e = \begin{cases} \emptyset, & \text{if } e \text{ is not close to } p_i \text{ (Def. 1)} \\ [\tau_1, t_{i+w-1}], & \text{if } t_i \leq \tau_1 \wedge t_i > \tau_1 - w_s \\ [t_i, \tau_2], & \text{if } \tau_1 < t_i \wedge t_i < \tau_2 \end{cases}$$

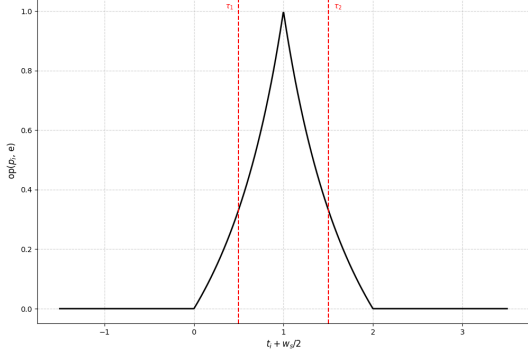


Fig. 1. Plot of  $op(p_i, e)$  as a function of  $t_i + w_s/2$ , the middle time of partition  $p_i$ .

To simplify, we define  $I_1 = ]\tau_1 - w_s, \tau_1]$  and  $I_2 = ]\tau_1, \tau_2[$ .

$$p_i \cup e = \begin{cases} [t_i, \tau_2], & \text{if } t_i \in I_1 \\ [\tau_1, t_i + w_s - 1], & \text{if } t_i \in I_2 \end{cases}$$

Based on the definitions, we can express  $op(p_i, e)$  as follows:

$$op(p_i, e) = \begin{cases} 0, & \text{if } e \text{ is not close to } p_i \\ \frac{t_i + w_s - \tau_1}{\tau_2 - t_i}, & \text{if } t_i \in I_1 \\ \frac{\tau_2 - t_i}{\tau_2 - t_i}, & \text{if } t_i \in I_2 \end{cases}$$

It is readily apparent that when  $t_i = \tau_1$ ,  $op(p_i, e)$  equals 1. Similarly, when  $t_i = \frac{\tau_1 + \tau_2}{2}$ ,  $op(p_i, e)$  equals  $\frac{1}{3}$ . Fig. 1 provides a visual representation of how  $op(p_i, e)$  changes with respect to the middle time of  $p_i$ , denoted as  $t_i + \frac{w_s}{2}$ . From the plot, it can be observed that the peak of  $op(p_i, e)$  is situated at the midpoint of event  $e$ .

**Definition 3.** We now define the  $op$  value of  $p_i$  with respect to all the events  $E$  as follows [23]:

$$op(p_i) = \max_{e \in E} op(p_i, e). \quad (2)$$

This definition suggests that  $op(p_i)$  is equivalent to  $op(p_i, e)$ , where  $e$  denotes the event that is closest to  $p_i$ . This is because the event closest to  $p_i$  exhibits the maximum overlap with the partition  $p_i$ .

**Definition 4.** We introduce a new function  $\pi : \mathcal{V} \rightarrow [0, 1]$  defined as follows:

$$\pi(v_i) : v_i \mapsto \pi(v_i) = op(p_i)$$

where  $p_i$  is a partition corresponding to  $v_i$ .

The function  $\pi$  is characterized as a black-box function, which means that there is no explicit mathematical formulation available for it. It's important to note that by selecting a sufficiently large value for  $w$ , we can ensure a one-to-one

correspondence between each  $v_i$  in  $\mathcal{V}$  and a unique  $p_i$  in  $\mathcal{P}$ . This is without loss of generality, as assuming that the function  $o$  is bijective allows us to associate  $v_i$  with  $p_i$  having the same index in the definition of the  $\pi$  function. This assumption of bijectivity simplifies the association process. The function  $\pi$  plays a pivotal role in the event detection process, a topic that will be further elaborated in the following sections.

### III. PRINCIPLE OF EVENT DETECTION

The principle of event detection, which employs overlapping partitions  $\mathcal{P}$  and the function  $\pi$ , revolves around finding a function  $f$  with a well-defined mathematical expression that accurately approximates the function  $\pi$ . A straightforward approach is to train a feed-forward neural network  $f$  on the set  $\{(v_i, \pi(v_i)) | i \in I_{train} \subset I\}$ . The approximation error for  $f$  is computed as:

$$\varepsilon(f) = \frac{1}{|I_{train}|} \sum_{i \in I_{train}} \mathcal{L}(f(v_i), \pi(v_i))$$

Here,  $\mathcal{L}$  denotes the loss function, which measures the disparity between the approximation value  $f(v_i)$  and the ground truth value  $\pi(v_i)$ . In regression problems, the mean squared error (MSE) is commonly employed as the loss function. Once trained,  $f$  can be applied to any vector  $v_k$  for  $k \in I_{test} \subset I$  to estimate  $\pi(v_k)$ , equivalent to  $op(p_k)$ . The peaks in  $op(p_k)$  for  $k \in I_{test}$  should align with the mid-times of the predicted events as illustrated previously in Fig. 1. These peaks are identified and analyzed to extract the predicted events, characterized by the intervals:

$$e_q = \left[ \tau_q - \frac{w_s}{2}, \tau_q + \frac{w_s}{2} \right]$$

Here,  $\tau_q$  denotes the mid-time of the  $q$ -th peak.

**Theorem 1.** If  $T$  and  $T^{-1}$  are continuous, then there exists a feed-forward neural network  $f \in \Sigma^r(\Psi)$  that utilizes a squashing function  $\Psi$ . This network can approximate the function  $\pi$  from  $\mathcal{V}$  to  $[0, 1]$  with arbitrary precision, given a sufficient number of hidden units  $Q$ .

A squashing function  $\Psi$  is a type of function that compresses the input into a smaller range. In neural networks, squashing functions, such as the sigmoid and hyperbolic tangent ( $\tanh$ ), serve as activation functions. These functions transform any input value into a range between 0 and 1 (for sigmoid) or between -1 and 1 (for  $\tanh$ ).

Here,  $\Sigma^r(\Psi)$  represents a set of single hidden layer feed-forward neural networks defined as follows:

$$\{f : \mathbb{R}^r \rightarrow \mathbb{R} : f(x) = \sum_{j=1}^Q \beta_j \Psi(A_j(x))\}$$

where  $x \in \mathbb{R}^r$ ,  $\beta_j \in \mathbb{R}$ , and  $A_j \in \mathbf{A}^r$ . The function  $A_j(x) = w_j \cdot x + b_j$ , with  $w_j \in \mathbb{R}^r$  and  $b_j \in \mathbb{R}$ . The parameters  $w_j, b_j$ , and  $\beta_j$  correspond to the network weights.

The proof for Theorem 1 is provided in the Appendix.

Under the continuity of both  $T$  and  $T^{-1}$ , Theorem 1 ensures that the function  $\pi$  can be effectively approximated by a feed-forward network  $f \in \Sigma^r(\Psi)$  with a sufficient number of

hidden units, providing precision to the desired degree. This establishes the foundation for our reliable and effective method in accurately detecting a wide range of events in time series data, as discussed in the earlier principles of detection.

It is important to note that the theoretical guarantees of the effectiveness and universality of our method are contingent on both the time series and its inverse being continuous. However, in practical scenarios where continuity conditions may not hold, our method remains effective based on the empirical success of neural networks in various applications. Neural networks have proven their ability to learn and approximate complex patterns, even in the absence of strict continuity assumptions. Therefore, while the theoretical guarantees assume continuity, the adaptability and learning capability of neural networks allow our framework to perform well in practice, accommodating scenarios where continuity conditions are relaxed.

Our method holds significant value for applications in signal processing, anomaly detection, and prediction across various fields, including finance, medicine, and engineering.

#### A. Practical Considerations

1) *Post-Processing for Noise Reduction*: Practical applications of feed-forward neural networks for regression tasks often introduce noise into predictions due to factors such as complex data, overfitting, and training limitations. In our scenario, the noise in predictions generated by  $f \in \Sigma^r(\Psi)$  can pose challenges when estimating peak locations, potentially leading to false events. To address this, *EventDetector* package incorporates a smoothing mechanism for the values of  $f$  by convolving it with a Gaussian kernel. This convolution operation reduces high-frequency noise while preserving the fundamental shape of  $f$ , enhancing the accuracy and reliability of peak location estimation, and reducing the occurrence of false events. The extent of smoothing is governed by the standard deviation  $\sigma$ . Optimal smoothing outcomes require selecting the optimal standard deviation. This is achieved using an optimization algorithm determining the value of  $\sigma$  maximizing the F1-Score [23]. Additionally, optimizing the peak threshold is essential to complement the smoothing process. The peak threshold determines which values in the smoothed  $f$  are considered as peaks. A suitable threshold ensures a balance between capturing ground truth peaks and minimizing the inclusion of noise-induced peaks. Similar to the standard deviation, optimizing the peak threshold is crucial for accurate peak detection results [23].

2) *Analysis of Peak Uncertainty*: Identified peaks are cross-referenced with peaks of ground truth events in the test set. A predicted peak is considered a match if it occurs within a maximum specified time tolerance  $\delta(t) \leq w_s$  of its corresponding ground truth peak. This time tolerance introduces flexibility in aligning predicted and actual event times, accounting for inherent temporal uncertainty in dataset labeling. Consequently, we construct a histogram of time differences between predicted and ground truth events to analyze the distribution of uncertainties.

## IV. NUMERICAL STUDY

In this section, we conduct a comprehensive evaluation of our method’s effectiveness on two challenging and imbalanced datasets. The first dataset focuses on credit card fraud detection [29], while the second dataset involves the detection of bow shock crossings in physical time series of plasmas. We employ the F1-Score metric, which adeptly balances precision and recall, making it particularly suited for assessing performance on imbalanced datasets where the minority class holds significant interest. Our method is implemented using the *EventDetector* Python package [23]. We benchmark our F1-Score results against state-of-the-art metrics obtained by diverse architectures, as reported in reputable literature [31]–[34]. All results and materials from this section are available on our GitHub repository for reproducibility: <https://github.com/menouarazib/eventdetector/>.

### A. Fraud Detection

1) *Setup*: The credit card fraud detection dataset labels each one-second time step as either 0 or 1, indicating the absence or presence of fraud, respectively. However, our method requires fraud instances to be represented as a list of time intervals. To reconcile this, we transform the labeled time steps corresponding to fraud occurrences into a list of time intervals. For each time step  $c_{1_q}$  where the label is 1 (indicating fraud), with the total number of frauds denoted as  $n_b$ , we define an interval as follows:

$$e_q = \left[ c_{1_q} - \frac{w_s}{2}, c_{1_q} + \frac{w_s}{2} \right]$$

Subsequently, we construct the list of fraud intervals:

$$E = \{e_q \mid q = 1, 2, \dots, n_b\}$$

Given that the fraud dataset has time steps of one second, i.e.,  $s = 1$  second, and considering that the deep learning methods we are comparing with ours are based on binary classification (predicting the presence or absence of fraud for each second), we need to ensure a fair comparison with our method. Therefore, we consider the temporal size  $w_s$  of fraud to be 1 second, which is specified by  $w_s = (w - 1) \cdot s$ . Thus, we must set  $w = 2$ . For our method, we use an FFN with a single hidden layer containing  $Q = 20$  neurons. The activation function  $\Psi$  is set to sigmoid and the partition size  $w$  is chosen to be 2.

2) *Comparison without Data Balancing (SMOTE)*: We begin by comparing our method with a deep learning approach that does not use any data balancing technique, such as SMOTE [30]. The benchmark method employs a Convolutional Neural Network (CNN) [31] on the imbalanced dataset.

TABLE I  
COMPARISON OF OUR METHOD WITH DEEP LEARNING METHOD WITHOUT SMOTE

Method	Number of Parameters	Precision	Recall	F1-Score
CNN [31]	119,457	0.89	0.68	0.77
Ours	1,201	0.98	0.74	0.85

Notably, our method demonstrates superior performance compared to the CNN-based method [31] across all metrics. Furthermore, our approach exhibits a substantial reduction in parameters, with 1,201 parameters as opposed to 119,457 in the CNN-based method. This significant parameter reduction not only indicates computational efficiency but also renders our method well-suited for scenarios with limited computational resources.

3) *Comparison with Data Balancing (SMOTE)*: Next, we compare our method with other deep learning methods that utilize SMOTE to balance the dataset before feeding it into a neural network. We consider the works by [32], [33], which used feed-forward neural networks with different architectures.

TABLE II  
COMPARISON OF OUR METHOD WITH DEEP LEARNING METHODS WITH SMOTE

Method	Number of Parameters	Precision	Recall	F1-Score
FFN+SMOTE [32]	5,561	0.79	0.81	0.80
FFN+SMOTE [33]	N/A	0.82	0.79	0.81
Ours	1,201	0.98	0.74	0.85

Table II illustrates that our method surpasses both competing methods that used SMOTE in terms of precision and F1-Score, achieving high performance even without using SMOTE for data balancing. Moreover, our method’s efficiency is evident in its significantly lower number of parameters, demonstrating its ability to achieve high performance with low complexity.

Fig. 2 presents a visual comparison between the predicted  $op$  values and the ground truth  $op$  values. The shape of the predicted values aligns well with the ground truth values, and occasional additional peaks may appear. The effectiveness of using a peak threshold to eliminate false peaks, as explained above, is evident in the improved accuracy of predictions. Furthermore, a time difference  $\delta(t)$  between predicted and ground truth events has a mean equal to -0.15 seconds and a standard deviation of about 0.48 seconds implying that our method achieves precise event detection.

### B. Bow Shock Crossings Detection

In this section, we extend the evaluation of our method to a distinct imbalanced dataset explicitly designed for plasma’s physical time series with bow shock crossing events. The dataset is derived from Mars Express spacecraft (MEX) data using the AMDA software [35], with ground truth annotations for bow shock crossings provided by [36].

We compare our method with a study by [34], where the authors developed a deep learning approach for bow shock crossing detection using Cassini data and ResNet18 [37], a well-known deep CNN architecture. Despite the entirely different nature of our dataset, focusing on time series data rather than images, we choose to compare with [34] due to the absence of other bow shock detection studies using deep learning on time series data. Our aim is to demonstrate that our method, with a minimal number of parameters, can achieve metrics comparable to state-of-the-art architectures like ResNet18.

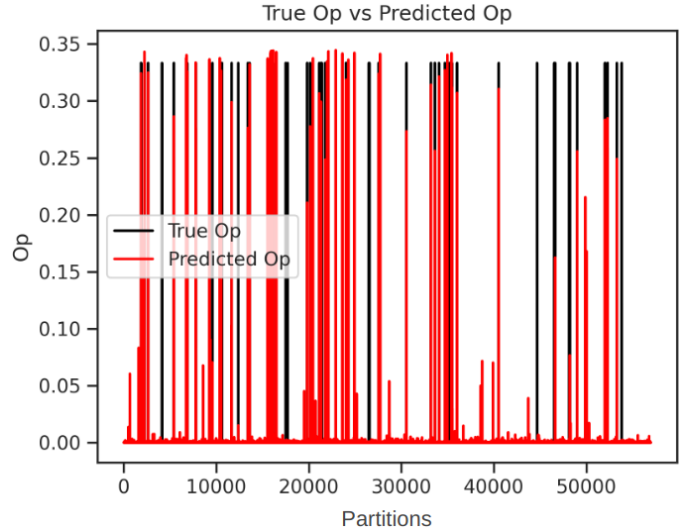


Fig. 2. Comparison between predicted and ground truth  $op$  values, demonstrating the effectiveness of peak thresholding in eliminating false peaks and improving prediction accuracy.

1) *Setup*: In configuring our approach, we intentionally selected a partition size  $w$  of 76. This decision aligns with the empirical understanding that a bow shock event typically spans 5 minutes, as indicated in [36], where criteria are assessed within a 5-minute timeframe to validate bow shock crossings. With our dataset’s sampling rate denoted by  $s$  and set at 4 seconds, the event duration  $w_s$  is precisely calculated as  $(76 - 1) \cdot 4 = 300$  seconds, corresponding to the acknowledged 5-minute duration.

In this specific configuration, we employ a feed-forward neural network featuring a single hidden layer. The hidden layer comprises  $Q = 20$  neurons and utilizes a sigmoid function as a squashing function.

2) *Performance Evaluation and Comparative Analysis*: Table III illustrates that our method surpasses the ResNet18-based method in terms of recall and F1-Score. Moreover, our method’s efficiency is evident in its significantly lower number of parameters, demonstrating its ability to achieve high performance with low complexity.

TABLE III  
COMPARATIVE ANALYSIS OF BOW SHOCK CROSSINGS DETECTION METHODS

Method	Number of Parameters	Precision	Recall	F1-Score
ResNet18 [34]	29,886,979	0.99	[0.83 , 0.88]	[0.91 , 0.94]
Ours	6,121	0.95	0.96	0.95

Fig. 3(a) illustrates the comparison between predicted  $op$  values and ground truth  $op$  values for the bow shock case. As expected, the predicted values closely align with the ground truth, exhibiting minimal fluctuations. Occasionally, additional peaks emerge, attributed to the benefits of peak threshold optimization in eliminating them.

In Fig. 3(b), the distribution of time differences  $\delta(t)$  between predicted events and ground truth events for the bow shock case is depicted. This visualization offers valuable insights

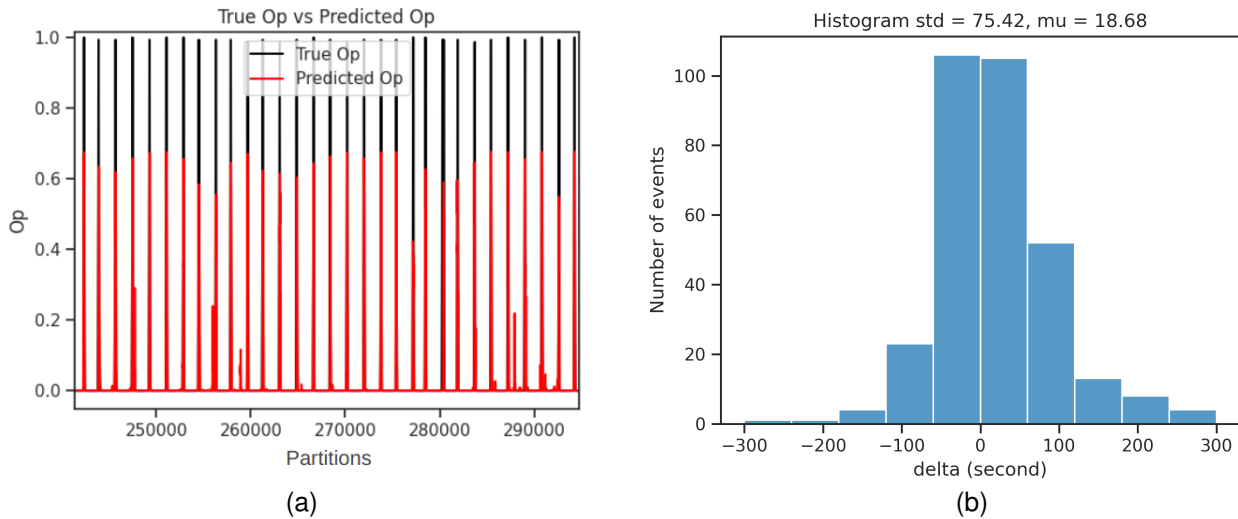


Fig. 3. (a) Comparison between predicted  $op$  ground truth  $op$  for the bow shock case. (b) Distribution of time differences  $\delta(t)$  between predicted events and ground truth events for the bow shock case.

into the temporal deviations between predicted and actual event occurrences, facilitating an analysis of the accuracy and precision of our event predictions concerning their temporal alignment. In this case, the distribution of time differences demonstrates a standard deviation of 75 seconds and a mean of 18 seconds. This indicates that predicted events typically deviate from ground truth events by an average of 18 seconds, with some variations of up to 75 seconds. This level of accuracy is noteworthy.

## V. EVENTDETECTOR PACKAGE

In addition to the theoretical considerations outlined earlier and incorporated into the *EventDetector* package, our package offers extensive configurations to cater to various study cases and optimize performance. Notably, users can leverage a range of options to customize the behavior of the event detection algorithm.

One notable configuration allows for the adjustment of the temporal duration of partitions, providing the flexibility to set it longer than the actual duration of events. This feature proves valuable when the objective is to capture a more extended context within each partition while maintaining a finer resolution for event detection. This configurational adaptability empowers users with a targeted approach to enhance precision in event detection.

Furthermore, the package incorporates a stacked ensemble learning approach, leveraging the combined strengths of multiple base models to elevate the accuracy and robustness of event detection [23]. This ensemble learning strategy enhances the overall performance of the *EventDetector* package, making it a versatile and powerful tool for event detection across diverse datasets and research domains. Users can benefit from these advanced configurations and techniques to tailor the package to their specific analytical needs and achieve optimal results in event detection scenarios.

## VI. CONCLUSION

In this paper, we have presented a theoretical foundation for our method of event detection in multivariate time series, which is based on regression rather than classification. We have demonstrated its universality under mild assumptions regarding the continuity of a multivariate time series. We have established that our approach can detect a broad spectrum of events with arbitrary precision, such as change points, frauds, anomalies, and more.

In addition to theoretical considerations, we have validated the practical efficacy of our approach. We have shown that with very few trainable parameters, our method outperforms existing deep-learning approaches on real-world imbalanced datasets, such as those used for fraud detection and bow shock crossing identification. These practical validations underscore the effectiveness and relevance of our method across various domains, thereby establishing it as a compelling solution for event detection in various fields.

However, it is essential to acknowledge that our method has certain limitations. Notably, multi-class event detection may not be straightforward.

As further work, we may also want to test our method on other different datasets from different fields, with a focus on obtaining state-of-the-art metrics on each dataset compared to other methods. This would allow us to highlight the benefits of our method, such as the small number of parameters needed to train it, which reduces the computational resources required and makes it a more sustainable and environmentally friendly solution.

## ACKNOWLEDGMENTS

This project was granted within the framework of the France Relance Program under the convention UT3 - N°0002890, which was supported by the French Ministère de l'Économie des Finances et de la Souveraineté Industrielle et Numérique. We like to thank Université Paul Sabatier Toulouse III, CNRS

for providing the computational infrastructure and hosting the Akkodis collaborator. Part of the analysis has been done by the AMDA software (<http://amda.cdpp.eu>) provided by CDPP (<http://www.cdpp.eu/>).

APPENDIX  
PROOF OF THEOREM 1

*Proof.* To prove Theorem 1, we first need to establish the continuity of the following three functions:  $o$ ,  $op$ , and  $\pi$ . But before delving into that, let's provide some definitions.

**Definition 5.** We define a metric  $d_{\mathcal{P}}$  as follows:

$$d_{\mathcal{P}} : \mathcal{P} \times \mathcal{P} \rightarrow \mathbb{R}$$

$$(p_i, p_j) \mapsto d_{\mathcal{P}}(p_i, p_j) = |t_i - t_j|$$

**Definition 6.** We define a metric  $d_{\mathcal{V}}$  as follows:

$$d_{\mathcal{V}} : \mathcal{V} \times \mathcal{V} \rightarrow \mathbb{R}$$

$$(v_i, v_j) \mapsto d_{\mathcal{V}}(v_i, v_j) = \sqrt{\sum_{m=1}^w \sum_{k=1}^f (T(t_{j+m-1})[k] - T(t_{i+m-1})[k])^2}$$

**Definition 7.** We define a metric  $d_T$  as follows:

$$d_T : \mathbb{R} \times \mathbb{R} \rightarrow \mathbb{R}$$

$$(t_i, t_j) \mapsto d_T(t_i, t_j) = \sqrt{\sum_{k=1}^f (T(t_j)[k] - T(t_i)[k])^2}$$

Consider  $0 < m \leq w$ ,  $i > 0$ ,  $j > i$ ,  $i, j \in I$ .

**Proving the Continuity of  $o$ :**

We have  $|t_{j+m-1} - t_{i+m-1}| = |t_j - t_i| = (j - i) \cdot s$ . Given  $\epsilon = s > 0$ , without loss of generality, assume  $s \ll 1$  (assuming  $N$  is sufficiently large). Then, there exists  $\delta = (j - i)\epsilon + \epsilon$  such that  $|t_{j+m-1} - t_{i+m-1}| < \delta$ . If we assume that the time series  $T$  is continuous, then  $|t_{j+m-1} - t_{i+m-1}| < \delta$  implies  $d_T(t_{j+m-1}, t_{i+m-1}) < \epsilon$ .

For  $p_i, p_j \in \mathcal{P}$ , let  $v_i = o(p_i)$  and  $v_j = o(p_j)$ . From the definition:

$$d_{\mathcal{V}}(v_i, v_j) = \sqrt{\sum_{m=1}^w \sum_{k=1}^f (T(t_{j+m-1})[k] - T(t_{i+m-1})[k])^2}.$$

If  $d_T(t_{j+m-1}, t_{i+m-1}) < \epsilon$ , then we can bound  $d_{\mathcal{V}}(v_i, v_j)$  as follows:

$$d_{\mathcal{V}}(v_i, v_j) < \sqrt{w}\epsilon.$$

Let  $\epsilon_1 = \sqrt{w}\epsilon$ . Choose  $\delta = (j - i)\frac{\epsilon_1}{\sqrt{w}} + \frac{\epsilon_1}{\sqrt{w}}$ . Now, if  $d_{\mathcal{P}}(p_i, p_j) < \delta$ , it implies  $d_{\mathcal{V}}(v_i, v_j) < \epsilon_1$ . Thus, we can conclude that  $o$  is continuous.

**Proving the Continuity of  $op$ :**

For  $p_i, p_j \in \mathcal{P}$ , we have  $d_{\mathcal{P}}(p_i, p_j) = (j - i) \cdot s$ . Assuming that  $s$  is very small (given  $N$  is sufficiently large), without loss of generality, let's consider  $s \ll 1$ . Under this assumption:

- $p_i$  and  $p_j$  share the same closest event  $e$ . Consequently, we express  $op(p_i)$  as  $op(p_i, e)$  and  $op(p_j)$  as  $op(p_j, e)$ .
- If  $t_i \in I_1$ , then  $t_j \in I_1$ , and if  $t_i \in I_2$ , then  $t_j \in I_2$ .

For  $t_j, t_i \in I_1$ , the bound for  $op(p_j) - op(p_i)$  is given by:

$$op(p_j) - op(p_i) < \frac{2d_{\mathcal{P}}(p_j, p_i)}{w_s}$$

Similarly, for  $t_j, t_i \in I_2$ , the bound is:

$$op(p_j) - op(p_i) > -\frac{2d_{\mathcal{P}}(p_j, p_i)}{w_s}$$

In summary:

$$|op(p_j) - op(p_i)| < \frac{2d_{\mathcal{P}}(p_j, p_i)}{w_s}$$

This relation is the Lipschitzian relation, implying the continuity of  $op$  [26].

**Proving the Continuity of  $\pi$ :**

Let  $(v_{i_n})_n$  be a sequence that converges to  $v_i$ , where  $v_i, v_{i_n} \in \mathcal{V}$ . This can be formally written as:

$$\lim_{n \rightarrow \infty} v_{i_n} = v_i$$

This means that as  $n$  approaches infinity, the sequence  $(v_{i_n})_n$  converges to  $v_i$ . In other words, the values of  $v_{i_n}$  get arbitrarily close to  $v_i$  as  $n$  gets larger and larger. These assignments are valid since the function  $o$  is continuous. For more on convergence sequences with continuous functions, please refer to [27].

Let's define  $v_i, v_{i_n}$  as follows:

$$v_i = \begin{pmatrix} x_i \\ \vdots \\ x_{i+w-1} \end{pmatrix}, v_{i_n} = \begin{pmatrix} x_{i_n} \\ \vdots \\ x_{(i+w-1)_n} \end{pmatrix}$$

Where  $x_{(i+k)_n}, x_{i+k} \in \mathbb{R}^f$ ,  $0 \leq k \leq w - 1$ . We have  $\lim_{n \rightarrow \infty} v_{i_n} = v_i \implies \lim_{n \rightarrow \infty} x_{(i+k)_n} = x_{i+k}$ ,  $0 \leq k \leq w - 1$  [28]. Since  $o$  is bijective, we can associate, for  $v_i, v_{i_n}$  respectively, the partitions  $p_i, p_{i_n}$  that can be defined as follows:

$$p_i = \{T^{-1}(x_{i+k}), 0 \leq k \leq w - 1\}$$

$$p_{i_n} = \{T^{-1}(x_{(i+k)_n}), 0 \leq k \leq w - 1\}$$

We have for  $0 \leq k \leq w - 1$  that  $\lim_{n \rightarrow \infty} x_{(i+k)_n} = x_{i+k}$  then if  $T^{-1}$  is continuous, we can deduce that:

$$\lim_{n \rightarrow \infty} p_{i_n} = p_i$$

Since  $op$  is continuous, then:

$$\lim_{n \rightarrow \infty} p_{i_n} = p_i \implies \lim_{n \rightarrow \infty} op(p_{i_n}) = op(p_i)$$

Finally, from the definition of the function  $\pi$ , we can write that  $\lim_{n \rightarrow \infty} v_{i_n} = v_i \implies \lim_{n \rightarrow \infty} \pi(v_{i_n}) = \pi(v_i)$ , thus  $\pi$  is continuous [28].

We have  $\mathcal{P}$  as a finite set, implying it is compact. Since  $o$  is continuous, the image of  $\mathcal{P}$  under  $o$ ,  $\mathcal{V}$ , is also compact [28]. Therefore,  $\pi$  is continuous over the compact set  $\mathcal{V}$ . According to Theorem 2.4 in [24], we can assert that a feed-forward neural network  $f \in \Sigma^r(\Psi)$ , utilizing a squashing function  $\Psi$ , can accurately approximate the function  $\pi$  with any desired degree of precision  $\lambda$ . In their proof, the authors of Theorem 2.4 in [24] choose the number of hidden units  $Q$  such that  $\frac{1}{Q} < \frac{\lambda}{2}$ , indicating that a larger value of  $Q$  is required to achieve an excellent approximation.  $\square$

## REFERENCES

- [1] M. A. Al-Masri and A. M. Al-Smadi, "A novel deep learning supervised method for event detection in multivariate time series data," *Scientific Programming*, vol. 2021, pp. 1-17, 2021, doi: 10.1155/2021/6636270.
- [2] C.-L. Chen, C. Rong, S. OuYang, and H. Sun, "Anomaly Detection in QAR Data Using VAE-LSTM with Multihead Self-Attention Mechanism," *Mobile Information Systems*, vol. 2022, p. 8378187, 2022. [Online]. Available: <https://doi.org/10.1155/2022/8378187>.
- [3] A. Reyana, S. Kautish, I. S. Yahia, and A. W. Mohamed, "MTEDS: Multivariate Time Series-Based Encoder-Decoder System for Anomaly Detection," *Computational Intelligence and Neuroscience*, vol. 2022, p. 4728063, 2022. [Online]. Available: <https://doi.org/10.1155/2022/4728063>
- [4] P. Mobtahej, X. Zhang, M. Hamidi, and J. Zhang, "An LSTM-Autoencoder Architecture for Anomaly Detection Applied on Compressors Audio Data," *Computational and Mathematical Methods*, vol. 2022, p. 3622426, 2022. [Online]. Available: <https://doi.org/10.1155/2022/3622426>.
- [5] S. Gopali, F. Abri, S. Siami-Namini, and A. S. Namin, "A Comparative Study of Detecting Anomalies in Time Series Data Using LSTM and TCN Models," *ArXiv*, vol. abs/2112.09293, 2021. [Online]. Available: <https://doi.org/10.48550/arXiv.2112.09293>.
- [6] Z. Zamanzadeh Darban, G. I. Webb, S. Pan, C. C. Aggarwal, and M. Salehi, "Deep Learning for Time Series Anomaly Detection: A Survey," *ArXiv*, vol. abs/2211.05244, 2022. [Online]. Available: <https://doi.org/10.48550/arXiv.2211.05244>.
- [7] R. Chalapathy, S. Chawla, "Deep Learning for Anomaly Detection: A Survey," *ArXiv*, vol. abs/1901.03407, 2019. [Online]. Available: <https://doi.org/10.48550/arXiv.1901.03407>.
- [8] K. Choi, J. Yi, C. Park, and S. Yoon, "Deep Learning for Anomaly Detection in Time-Series Data: Review, Analysis, and Guidelines," *IEEE Access*, vol. 9, pp. 120043-120065, 2021. [Online]. Available: <https://doi.org/10.1109/ACCESS.2021.3107975>.
- [9] Y. Su, Y. Zhao, C. Niu, R. Liu, W. Sun, and D. Pei, "Robust Anomaly Detection for Multivariate Time Series through Stochastic Recurrent Neural Network," *Proceedings of the 25th ACM SIGKDD International Conference on Knowledge Discovery & Data Mining - KDD '19*, 2019. [Online]. Available: <https://doi.org/10.1145/3292500.3330672>.
- [10] D. Li, D. Chen, J. Goh, and S. Ng, "Anomaly Detection with Generative Adversarial Networks for Multivariate Time Series," *arXiv preprint arXiv:1809.04758*, 2019. [Online]. Available: <https://doi.org/10.48550/arXiv.1809.04758>.
- [11] X. Xu, H. Zhao, H. Liu and H. Sun, "LSTM-GAN-XGBOOST Based Anomaly Detection Algorithm for Time Series Data," 2020 11th International Conference on Prognostics and System Health Management (PHM-2020 Jinan), Jinan, China, 2020, pp. 334-339, doi: 10.1109/PHM-Jinan48558.2020.00066.
- [12] M. A. Bashar and R. Nayak, "TAnoGAN: Time Series Anomaly Detection with Generative Adversarial Networks," 2020 IEEE Symposium Series on Computational Intelligence (SSCI), Canberra, ACT, Australia, 2020, pp. 1778-1785, doi: 10.1109/SSCI47803.2020.9308512.
- [13] S. Han and S. S. Woo, "Learning Sparse Latent Graph Representations for Anomaly Detection in Multivariate Time Series," in *Proceedings of the 28th ACM SIGKDD Conference on Knowledge Discovery and Data Mining (KDD '22)*, Association for Computing Machinery, New York, NY, USA, 2022, pp. 2977-2986, doi: 10.1145/3534678.3539117.
- [14] S. Oswal, S. Shinde, and M. Vijayalakshmi, "A Survey of Statistical, Machine Learning, and Deep Learning-Based Anomaly Detection Techniques for Time Series," in *Advanced Computing*, D. Garg, V. A. Narayana, P. N. Suganthan, J. Anguera, V. Koppula, and S. K. Gupta, Eds., Springer Nature Switzerland, Cham, 2023, pp. 221-234, doi: 10.1007/978-3-031-35644-5\_17.
- [15] H. Du and Z. Duan, "Finder: A novel approach of change point detection for multivariate time series," in *Applied Intelligence*, vol. 52, pp. 2496-2509, 2022, doi: 10.1007/s10489-021-02532-x.
- [16] S. Oehmcke, O. Zielinski, and O. Kramer, "Event Detection in Marine Time Series Data," in *KI 2015: Advances in Artificial Intelligence*, S. Hölldobler, R. Peñaloza, and S. Rudolph, Eds. Cham: Springer International Publishing, 2015, pp. 279-286.
- [17] S. Aminikhanghahi and D. J. Cook, "A survey of methods for time series change point detection," *Knowl. Inf. Syst.*, vol. 51, no. 2, pp. 339-367, May 2017, doi: 10.1007/s10115-016-0987-z.
- [18] M. Gupta, R. Wadhvani, and A. Rasool, "Real-time change-point detection: A deep neural network-based adaptive approach for detecting changes in multivariate time series data," *Expert Syst. Appl.*, vol. 209, p. 118260, 2022, doi: 10.1016/j.eswa.2022.118260.
- [19] J. Li, P. Fearnhead, P. Fryzlewicz, and T. Wang, "Automatic Change-Point Detection in Time Series via Deep Learning," *arXiv preprint arXiv:2211.03860*, 2023.
- [20] P. Granjon, "The CuSum algorithm - a small review," HAL Id: hal-00914697, 2014.
- [21] P. L. Bartlett, N. Harvey, C. Liaw, and A. Mehrabian, "Nearly-tight VC-dimension and Pseudodimension Bounds for Piecewise Linear Neural Networks," *Journal of Machine Learning Research*, vol. 20, no. 63, pp. 1-17, 2019. [Online]. Available: <http://jmlr.org/papers/v20/17-612.html>.
- [22] S. Jewell, P. Fearnhead, and D. Witten, "Testing for a Change in Mean after Changepoint Detection," *J. R. Stat. Soc. Ser. B. Stat. Methodol.*, vol. 84, no. 4, pp. 1082-1104, 2022, doi: 10.1111/rssb.12501.
- [23] M. Azib, B. Renard, P. Garnier, V. Génot, and N. André, "A Comprehensive Python Library for Deep Learning-Based Event Detection in Multivariate Time Series Data and Information Retrieval in NLP," *arXiv preprint arXiv:2310.16485*, 2023.
- [24] K. Hornik, M. Stinchcombe, and H. White, "Multilayer feed-forward networks are universal approximators," *Neural Networks*, vol. 2, no. 5, pp. 359-366, 1989, doi: [https://doi.org/10.1016/0893-6080\(89\)90020-8](https://doi.org/10.1016/0893-6080(89)90020-8).
- [25] P. Jaccard, "Etude de la distribution florale dans une portion des Alpes et du Jura," *Bulletin de la Societe Vaudoise des Sciences Naturelles*, vol. 37, pp. 547-579, Jan. 1901. doi: 10.5169/seals-266450.
- [26] S. Cobzas, R. Miculescu and A. Nicolae, "Lipschitz Functions: Theory and Applications," 1st ed., vol. 2241, Cham, Switzerland: Springer, 2019.
- [27] M. J. Hoffman, "Continuity of Inverse Functions," in *Mathematics Magazine*, vol. 48, no. 2, pp. 66-73, 1975. Accessed on: Nov. 16, 2023. [Online]. Available: <https://doi.org/10.2307/2689822>.
- [28] W. Rudin, "Principles of Mathematical Analysis," Taibei Shi, Taiwan: Zhong yang tu shu chu ban she, 1967.
- [29] I. Benchaji, S. Douzi, and B. E. Ouahidi, "Credit card fraud detection model based on LSTM recurrent neural networks," *J. Adv. Inf. Technol.*, vol. 12, no. 2, pp. 113-118, 2021, doi: 10.12720/jait.12.2.113-118.
- [30] N. V. Chawla, K. W. Bowyer, L. O. Hall and W. P. Kegelmeyer, "SMOTE: Synthetic Minority Over-sampling Technique," in *Journal of Artificial Intelligence Research*, vol. 16, pp. 321-357, 2002.
- [31] F. K. Alarfaj, I. Malik, H. U. Khan, N. Almusallam, M. Ramzan and M. Ahmed, "Credit Card Fraud Detection Using State-of-the-Art Machine Learning and Deep Learning Algorithms," in *IEEE Access*, vol. 10, pp. 39700-39715, 2022, doi: 10.1109/ACCESS.2022.3166891.
- [32] D. Varmedja, M. Karanovic, S. Sladojevic, M. Arsenovic and A. Anderla, "Credit Card Fraud Detection - Machine Learning methods," 2019 18th International Symposium INFOTEH-JAHORINA (INFOTEH), East Sarajevo, Bosnia and Herzegovina, 2019, pp. 1-5, doi: 10.1109/INFOTEH.2019.8717766.
- [33] E. Ileberi, Y. Sun and Z. Wang, "A machine learning based credit card fraud detection using the GA algorithm for feature selection," in *J Big Data*, vol. 9, no. 24, 2022. [Online]. Available: <https://doi.org/10.1186/s40537-022-00573-8>.
- [34] I. K. Cheng, N. Achilleos and A. Smith, "Automated bow shock and magnetopause boundary detection with Cassini using threshold and deep learning methods," *Front. Astron. Space Sci.*, vol. 9, 2022, doi: 10.3389/fspas.2022.1016453.
- [35] V. Génot et al., "Automated multi-dataset analysis (amda): An online database and analysis tool for heliospheric and planetary plasma data," *Planetary and Space Science*, vol. 201, 105214, Apr. 2021. doi: 10.1016/j.pss.2021.105214.
- [36] B. E. S. Hall et al., "Annual variations in the Martian bow shock location as observed by the Mars Express mission," *J. Geophys. Res. Space Phys.*, vol. 121, no. 11, pp. 11,474-11,494, Nov. 2016, doi: 10.1002/2016JA023316.
- [37] K. He, X. Zhang, S. Ren, and J. Sun, "Deep Residual Learning for Image Recognition," *arXiv:1512.03385 [cs.CV]*, Dec. 2015.